3D Hollow ZnO Spheres Embedded withTiO$_2$ Nanoparticles as Anodes for High-Performance of Lithium-ion Batteries

Xiaona Zhao[1], Ziying Zhang[1,*], Huizhen Zhang[2], Xingran Xu[1], Xuanxuan Fan[1], Sijia Wang[1]

[1] School of Materials Engineering, Shanghai University of Engineering Science, Shanghai 201620, China
[2] School of Management, University of Shanghai for Science and Technology, Shanghai 200093, China
[*]E-mail: zzying@sues.edu.cn

Despite ZnO was considered as an ideal anode material for lithium-ion batteries owing to its high theoretical capacity, the defects of its conductivity and volume expansion hinder its further development in the field of energy storage. Under the guidance of the synergistic effect of the two materials, 3D hollow ZnO/TiO$_2$ composite spheres were fabricated by solvothermal method and low temperature hydrolysis. The unique hollow porous structure highlighted a large specific surface area and promoted the transport of lithium ions. TiO$_2$ nanoparticles closely embedded in the voids of porous hollow ZnO spheres, which effectively improved the structural stability of the final products during charge and discharge. The 3D hollow ZnO/TiO$_2$ composite sphere electrodes exhibited a good cycling stability. Their discharge capacity stabilized at 709 mA hg^{-1} at current density of 500 mA g^{-1} after 500 cycles. Even at the high current density of 1000 mA g^{-1}, their discharge capability remained at 540 mA h g^{-1}, showing a good application prospect.

1. INTRODUCTION

As a promising energy storage device, rechargeable lithium ion batteries (LIBs) have be widely used in new energy vehicles, smart grids and flexible electronic devices, and have gradually become one of the indispensable things in People's Daily life.[1-3] However, with the rapid development of hybrid electric vehicles and electronic products, traditional graphite materials are unable to meet the demands of high energy density and long-term cycle life due to its low theoretical capacity and poor rate capability.[4,5] In order to replace graphite, transition metal oxides with high difusion coefcient and large capacity in lithium-ion battery anode materials have been extensively studied.[6-10]

As a metal oxide, ZnO is an ideal anode material with high theoretical capacity (~ 1000 mA h g^{-1}), highly electrical conductivity and environmental compatibility.[11,12] However, the application of ZnO as anode material was limited due to its large volume expansions and poor electronic conductivity.[13-15] Recently, numerous strategies have been employed to address these bottlenecks, including the preparation of different nanostructure, porous carbon coatings, and creating composites from other stable oxides.[16-20] Despite the fact that the offered larger interfacial area, shrinking mechanical deformation and good electrochemical performances, significant volume fluctuations still needed to be improved during the cycling process. Compared with ZnO, TiO_2 was considered to be another attractive anode material for lithium ion batteries due to its good environmental friendliness and structural stability.[21,22] However, it has a theoretical capacity of 335 mA h g^{-1}, similar to graphite.[23,24] Therefore, TiO_2 was mainly used as a decorative material for composite materials to promote the electrochemical performance of the electrode.[25] In order to improve the electrochemical performance of ZnO, Gao et al.[26] prepared 3D interconnected TiO_2@ZnO nano-arrays by uniformly growing ZnO nanoparticles on TiO_2 nanosheet arrays to alleviate the volume change and aggregation of ZnO nanoparticles. Recently, we have successfully synthesized TiO_2@ZnO hollow nanoflower arrays with high-rate capability and long-term cycling performance by using TiO_2 as host material.[27] Inspired by the advantages of hollow porous nanospheres and the structural stability of TiO_2, the injection of TiO_2 nanoparticles into porous hollow ZnO spheres as a buffer medium was expected to be an effective strategy for the preparation of ZnO nanocomposite electrode materials with high structure stability and cycling stability.

Herein, novel 3D hollow ZnO/TiO_2 composite spheres were prepared by solvothermal method and low temperature hydrolysis method. The unique porous hollow structure highlighted a large specific surface area and promoted the transport of lithium ions. TiO_2 nanoparticles were tightly embedded into the voids of porous hollow ZnO spheres, which effectively improved the structural stability of the final products during charge and discharge. The discharge capacity of the hollow ZnO/TiO_2 composite sphere electrodes exhibited a slight decline at current density of 500 mA g^{-1} after 500 cycles. The idea of using the synergistic effect of the two materials will aid in the further development of high-performance lithium ion anode materials.

2. EXPERIMENTAL SECTION

2.1 Synthesis of ZnO porous hollow sphere

Porous ZnO spheres were prepared by the solvothermal method using zinc acetate as zinc source and anhydrous glucose as carbon source. First, 25 mmol anhydrous glucose ($C_6H_{12}O_6$), 12.5 mmol Zinc acetate dihydrate ($Zn(CH_3COO)_2 \cdot 2H_2O$), and 25 mmol carbamide ($CO(NH_2)_2$) were added to a 60 mL anhydrous alcohol-water mixture(the volume ratio is 5:1), and stirred at room temperature for 30 min. Then, the mixed solution was poured into a 100 ml Teflon-lined autoclave and maintained at 160 °C for 16 h. After the reactor was cooled to room temperature, the products were collected by centrifugation. To obtain white ZnO porous hollow spheres, the black products were further annealed at 900 °C for 3 h.

2.2 Synthesis of hollow ZnO/TiO$_2$ composite spheres

Hollow ZnO/TiO$_2$ spheres were prepared by low temperature hydrolysis. 0.5 g porous hollow ZnO spheres were immersed in a mixture of aqueous ethanol solution and deionized water (vol, 20:1), 23 ul tetrabutyl titanate was added, and fully stirred at 4 °C for 24h. After the reaction, the products were centrifugally washed with ethanol and deionized water and dried at 60 °C. Finally, hollow ZnO/TiO$_2$ spheres were obtained by annealing at 450 °C for 5 h in argon.

2.3 Material Characterizations

The microstructures of the samples were characterized by field emission scanning electron microscopy (SEM, Hitachi SU8010, Japan) and transmission electron microscope (TEM; JEOL 2100F). The crystal structure of the products was analyzed by Cu KαX-ray diffractometer. Chemical composition was analyzed by XPS (Thermo Fisher K-Alpha, America). The BET and BJH methods were used to calculate the specific surface area and porosity of the products, respectively.

2.4 Electrochemical Measurements.

The electrochemical properties of the prepared products were determined by using lithium tablets as counter electrode. The electrode slurry was prepared by mixing active materials, conducting agent and PVDF with a mass ration of 7:2:2 and coated on copper foil to form electrode slices.The CR2032 coin cells were assembled in a vacuum glove box with the dried electrode slices as cathodes, polypropylene microporous membrane as separators, 1M LiPF6 EC/DMC(1:1) solution as electrolyte. Galvanostatic charge-discharge tests were carried out with NeYAR-CT300 cell tester within the voltage window of 0.01-3V (vs Li/Li+) at room temperature. A cyclic voltammetric (CV) curves can be obtained at a scanning rate of 0.1 mV s^{-1} in the potential range from 0.01 to 3.00 V. The electrical impedance spectra (EIS) measurements were performed in the frequency range of 100 kHz to 0.01 Hz. The PARSTAT-4000 electrochemical workstation was used to test the CV and EIS measurements.

3. RESULTS AND DISCUSSION

3.1. Synthesis and characterization

Figure 1a is a detailed schematic diagram of the synthesis process of hollow ZnO/TiO$_2$ spheres. First, Zinc oxide precursor was synthesized by solvothermal method with glucose (C$_6$H$_{12}$O$_6$), carbamide (CO(NH$_2$)$_2$) and zinc acetate dihydrate (Zn(CH$_3$COO)$_2$·2H$_2$O) as raw materials. Porous hollow ZnO spheres were prepared by high temperature annealing. Then, TiO$_2$ nanospheres were embedded into the voids of porous hollow ZnO spheres by hydrolysis and calcination of tetrabutyl titanate. The implanted TiO$_2$ nanospheres were expected to alleviate the volume expansion of ZnO nanoparticles during the charging and discharging process.
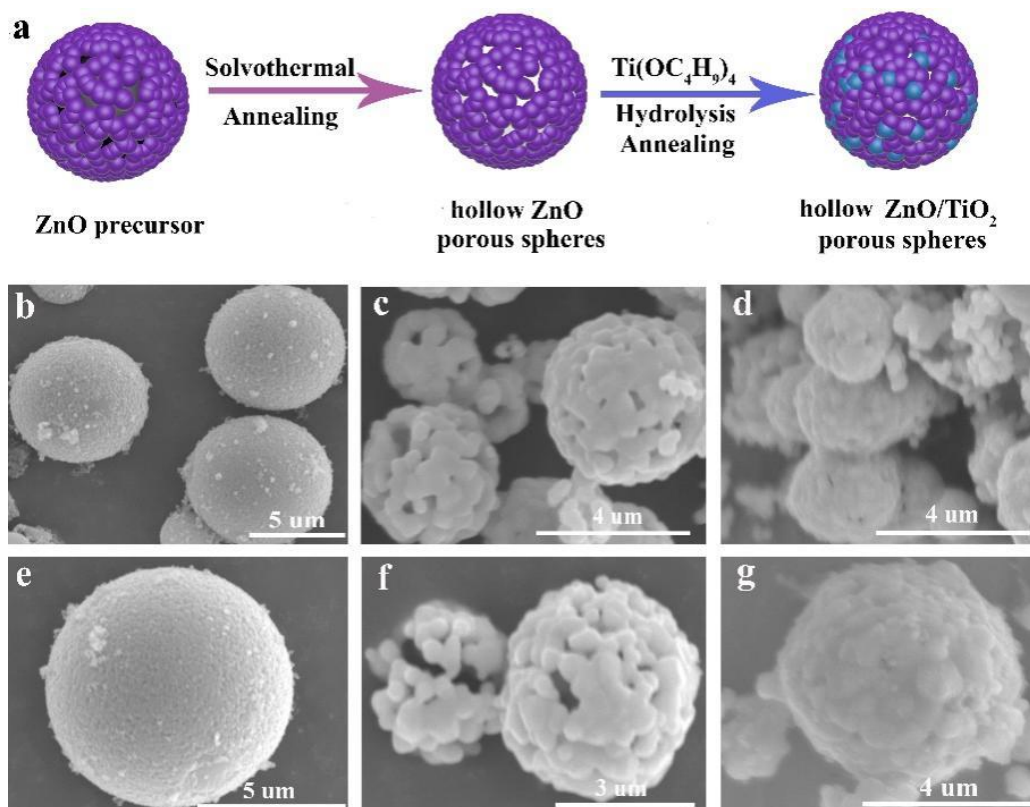
Figure 1. (a) Schematics fabrication process of hollow ZnO/TiO$_2$ composite spheres, SEM images of (b, e) ZnO precursor, (c, f) hollow ZnO porous spheres, (d, g) hollow ZnO/TiO$_2$ composite spheres.

Figure 1b and 1e show SEM images of the ZnO precursors. The ZnO precursors had a spherical structure and no obvious agglomeration phenomenon. They were uniform in size, about 7 um in diameter. After dehydration reaction and and decarbonization reaction at 900°C, the ZnO precursors polycondensated into porous hollow ZnO spheres with an average diameter of about 4um, which was smaller than their precursors (Figure 1c and 1f). The shell of the hollow ZnO spheres was composed of 0.5 um nanoparticles. The surface of hollow ZnO spheres appeared an obvious cavitation phenomenon due to the condensation of ZnO precursors. After hydrolysis and calcination of tetrabutyl titanate, TiO$_2$ nanoparticles filled the voids and formed hollow ZnO/TiO$_2$ composite spheres with no significant size change (Figure 1d and 1g).
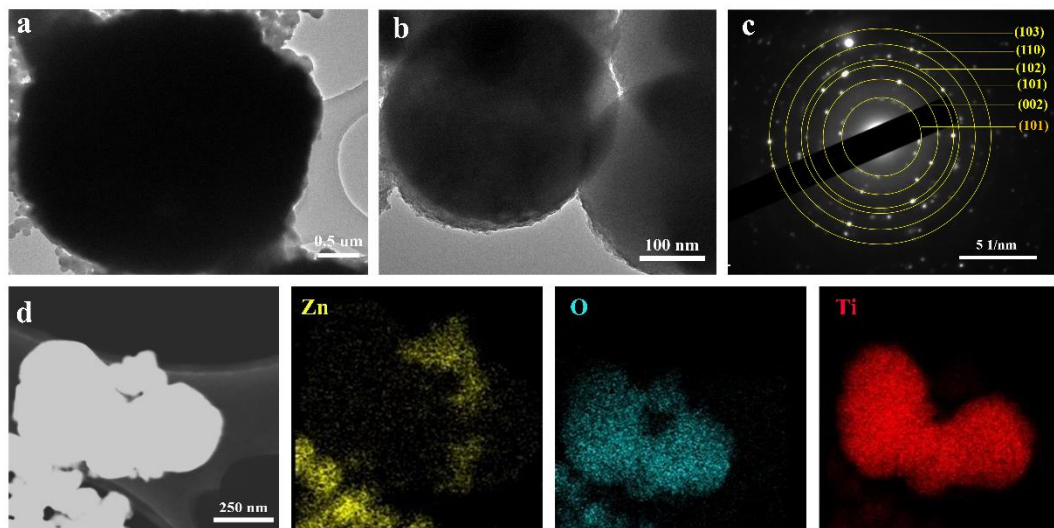
Figure 2. TEM and HRTEM images of hollow ZnO/TiO$_2$ composite spheres: (a) TEM image, (b) HRTEM image, (c) electron diffraction spectra, (d) EDX elemental mapping images

Figure 2 shows TEM images of ZnO/TiO$_2$ composite spheres. The homogeneity of center and edge indicated that the insertion of TiO$_2$ particles eliminated the obvious cavitation phenomenon in ZnO spherical shells (Figure 2a and 2b).
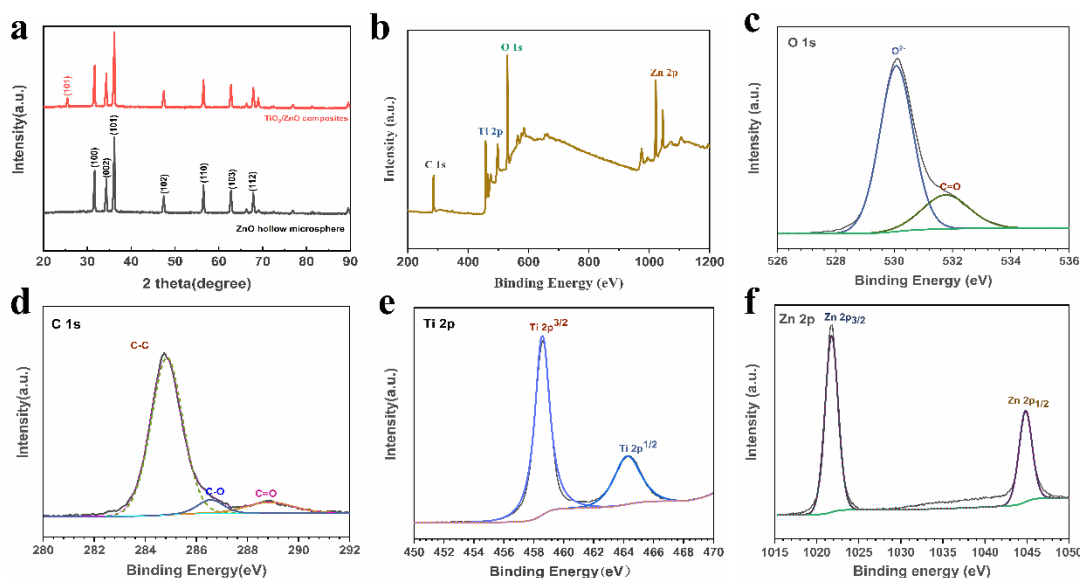
Figure 3. (a) XRD patterns of porous hollow ZnO spheres and hollow ZnO/TiO$_2$ composite spheres. XPS spectra of hollow ZnO/TiO$_2$ composite spheres: (b) survey spectra, (c) O 1s core-level spectra, (d) C 1s core-level spectra, (e) Ti 2p core-level spectra, (f)Zn 2p core-level spectra.

The electron diffraction patterns of continuous concentric circles in the selected area of the sample indicated that the composite spheres were polycrystalline (Figure 2c). The concentric ring closest

to the center of the SAED pattern was identified as the lattice plane of (101) of TiO_2. The EDS mapping showed that Ti element was surrounded by Zn and O elements, confirming that TiO_2 particles were successfully embedded into the voids of porous hollow ZnO spheres (Fig 2d).

Figure 3a shows the XRD patterns of the products. The diffraction peaks were consistent with ZnO phase (ICPDS no.05-0664). The diffraction peaks of porous hollow ZnO spheres were mainly located at 31.74°, 34.40°, 36.21°, 47.49°, 56.52°, 62.28°, 67.86°, corresponding to the lattice plane of (100), (002), (101), (102), (110), (103), (112), respectively. There were no other characteristic peaks on the curve, implying that ZnO hollow porous spheres had high purity and crystallinity. The diffraction peaks of hollow ZnO/TiO_2 composite spheres showed a small crystallization peak at $2\theta=25.2°$, which was the sign of (101) lattice planes in TiO_2 (ICPDS no.04-0477).[28] Here, the lower peak can be attributed to the lower TiO_2 content in the complex.

XPS further characterized the composition and valence states of hollow ZnO/TiO_2 composite spheres. It can be seen from the survey spectrum of ZnO/TiO_2 that there were no other peaks except Zn, Ti, O and C elements (Figure 3b). According to the high-resolution O 1s spectra (Figure 3c), the binding energy at 530.2eV and 531.7eV were ascribed to the combination of O^{2-} with Ti and Zn to form oxides and C=O bond.[29] Figure 3d shows that the XPS spectrum of C 1s presented three doublet component peaks. The peaks at 284.8, 286.5 and 288.6eV reflected the C-C, C-O-C and O-C=O bonds, respectively. The high resolution Ti 2p spectrum had two peaks at 458.5 and 464.3 eV, corresponding to Ti $2p^{3/2}$ and Ti $2p^{1/2}$(Figure 3e), respectively.[30] The splitting value between Ti $2p^{3/2}$ and Ti $2p^{1/2}$ was 5.8eV, which was a conventional characteristic of Ti^{4+} in anatase type TiO_2. The binding energy of Zn 2p spectrum at 1021.73 eV and 1044.67 eV were consistent with those of Zn $2p^{3/2}$ and Zn $2p^{1/2}$ in ZnO (Figure 3f).[31] All the results of XPS measurements show that the final product was a combination of ZnO and TiO_2.
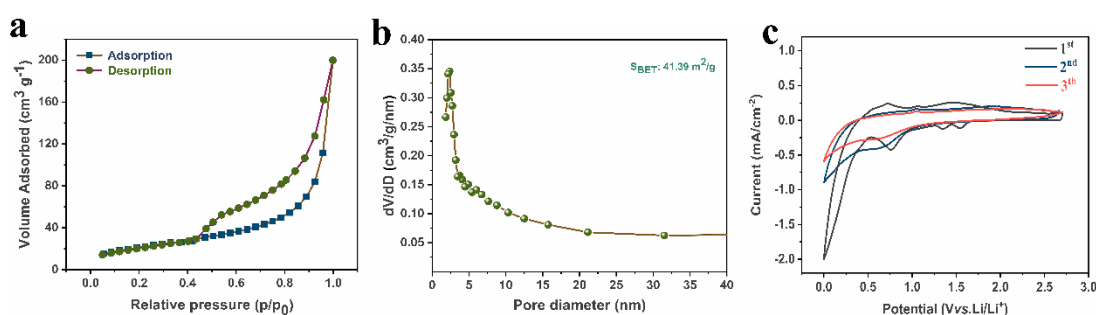
Figure 4. (a) Nitrogen adsorption-desorption isotherms. (b) pore size distribution of hollow ZnO/TiO_2 composite spheres. (c) CV curves of hollow ZnO/TiO_2 composite spheres.

In order to investigate the specific surface area and the pore size distribution of ZnO/TiO_2 composite hollow spheres, N_2 adsorption-desorption experiments were carried out. The typical IV isotherm in the N_2 adsorption−desorption isotherm curve (Figure 4a) indicated that the product was a mesoporous material. The specific surface area of ZnO/TiO_2 composite hollow spheres was 41.39 m^2 g^{-1}. Figure 4b shows that the pore size distribution of the sample was between 4 and 10nm. Hollow

ZnO/TiO₂ composite spheres had a large specific surface area, which significantly increased the contact area between the active materials and lithium ions. The mesoporous characteristics not only facilitate the migration of lithium ions, but also inhibit the volume change of the active materials during the insertion and separation of lithium ions, thus optimizing the cyclic stability of the final electrode.[32-34]

3.2. Electrochemical properties
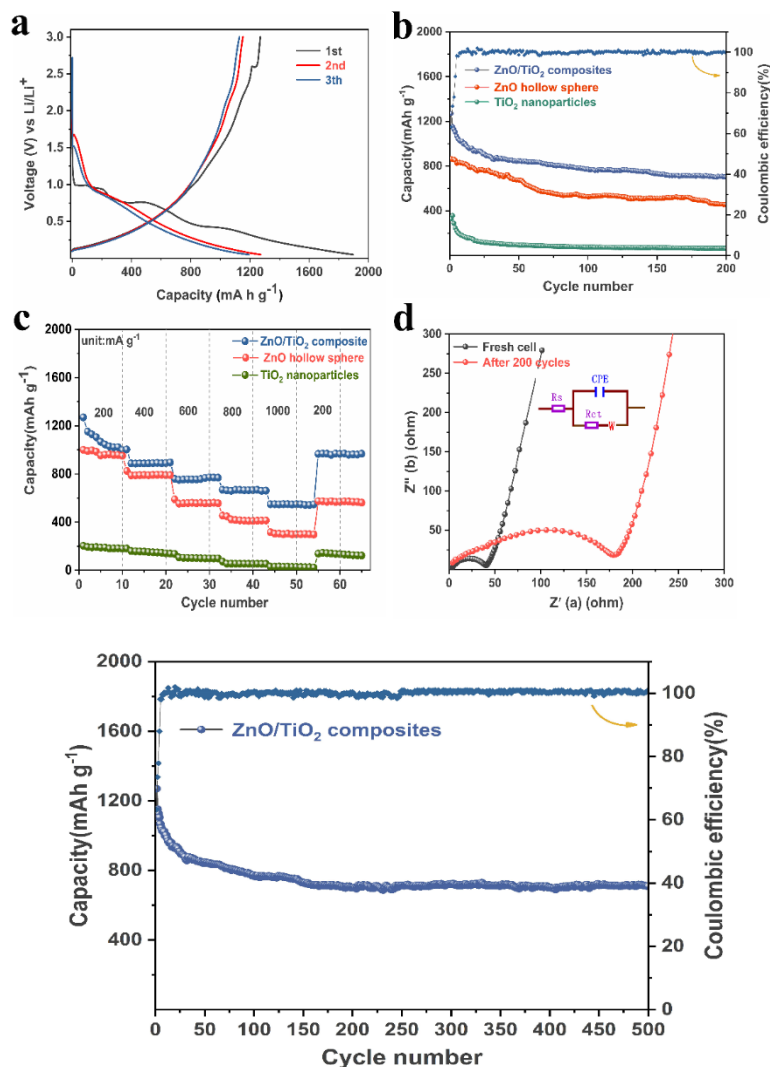
Figure 5. (a) Charge-discharge voltage profiles of hollow ZnO/TiO₂ composite spheres, (b) Cycling performances of hollow ZnO/TiO₂ composite spheres, ZnO hollow porous spheres and TiO₂ nanoparticles. (c)Rate performances of hollow ZnO/TiO₂ composite spheres, ZnO hollow porous spheres and TiO₂ nanoparticles. (d) Impedance analysis of hollow ZnO/TiO₂ composite spheres. (e) Cycling performance of hollow ZnO/TiO₂ composite sphere electrodes at 500 mA g^{-1} for 500 cycles.

The electrochemical properties of hollow ZnO/TiO₂ composite spheres were investigated with lithium tablet as a counter electrode. Figure 4c shows the first three CV curves of hollow ZnO/TiO₂

composite spheres at the sweep rate of 0.1 mV s^{-1}. On the first scan, there were three distinct peaks at 0.75, 1.35 and 1.56 V, respectively. The strong reduction peak near 0.75 V was caused by the alloying reaction of ZnO and weakened in the subsequent cycles, indicating that this was irreversible.[35] The two peaks at 1.35 V and 1.56 V were related to the formation of solid electrolyte interphase (SEI) layer and the transition from ZnO to Zn and Li_2O, respectively.[36] The two continuous small anodic peaks in the range of 0.25 ~ 0.75 V were the result of LiZn multi-step de-alloying reaction, and the oxidation peak at 1.5 V was a sign of ZnO resynthesis.[37-39] The good overlap of the subsequent cycles indicated that the obtained products possessed excellent structural stability and electrochemical reversibility.

Figure 5a shows the galvanostatic discharge-charge curves of hollow ZnO/TiO_2 composite spheres at current density of 500 mA g^{-1}. During the first discharge process, an distinct voltage platform could be observed at 0.9 V due to the formation of SEI.[40] This was consistent with the CV test results. In the first discharge-charge cycle, ZnO/TiO_2 hollow composite sphere electrodes exhibited a discharge capacity of 1897 mA h g^{-1} and charge capacity of 1270 mA h g^{-1}, corresponding a Coulomb efficiency of 67%. The irreversible loss of capacity was mainly caused by the irreversible chemical reaction.[41] After the first cycle, the charge-discharge capacity was stable at 1200 mA h g^{-1}, and the Coulomb efficiency was above 99%. Figure 5b shows the comparison of cycling performance of hollow ZnO/TiO_2 composite spheres, TiO_2 nanoparticles and hollow ZnO spheres at current density of 500 mA g^{-1}. Due to the particular structure and synergistic effect, the capacity of hollow ZnO/TiO_2 composite spheres was stable at 715 mA h g^{-1}, and the Coulomb efficiency remained above 99.5% after 200 cycles. In contrast, the capacity of ZnO porous spheres only retained 457.2 mA h g^{-1} after 200 cycles, which was about 50% lower than the initial discharge capacity. This was related to the lithium storage mechanism of ZnO. [42,43] Although TiO_2 nanoparticle electrodes could be circulated stably, due to its low theoretical capacity, the capacity after 200 cycles was only 164 mA h g^{-1}. Figure 5c shows the rate properties of three different materials. Hollow ZnO/TiO_2 composite spheres revealed good rate performance in the three materials. At current density of 200 mA g^{-1}, 400 mA g^{-1}, 600 mA g^{-1}, 800 mA g^{-1} and 1000 mA g^{-1}, their capacities were 1100, 890, 750, 660 and 540 mA h g^{-1}, respectively. Similar to TiO_2 nanoparticles, when the current density returned to 200 mA h g^{-1}, the discharge capacity was restored to 960 mA h g^{-1}, indicating that hollow ZnO/TiO_2 composite spheres exhibited good rate performance. In contrast, the discharge capacity of porous ZnO spheres decreased obviously with the increase of current density. When the current density was restored to 200 mA g^{-1}, the discharge capacity of porous ZnO spheres was only 570 mA h g^{-1}, which was about 57% of initial capacity. The results revealed that the hollow ZnO/TiO_2 composite spheres exhibited a good cycling performance due to their unique hollow structure and the synergistic effect of the two materials. Table 1 lists the comparison of electrochemical performance with previous literature. It can be seen that hollow ZnO/TiO_2 composite spheres exhibited better comprehensive performance in the same kind of composite materials due to their unique structural design.

Table 1. Comparison of ZnO/TiO_2 composites as anodes for lithium ion batteries

Materials	Type	Current density (mA g-1)	Cycle numbers	Specific capacity (mA h g-1)	References
ZnO/TiO_2 nanosheet	LIBs	200	100	340	[26]
$TiO_2@ZnO$ Hollow Nanoflower	LIBs	200	200	846	[27]
$TiO_2@ZnO$ nanorod	LIBs	50	30	447	[44]
ZnO/TiO_2 nanolaminates	LIBs	500	100	381	[45]
$ZnO/TiO_2/C$ nanofibers	LIBs	1000	300	392	[46]
This work	LIBs	500	500	709.5	

Figure 5d shows the EIS of hollow ZnO/TiO_2 composite sphere electrodes before and after cycling in the frequency range of 100 kHz to 0.01 Hz. All Nenquist plots consisted of a semicircle line and an oblique line, representing the high and low-frequency regions respectively. The diameter of the semicircle was mainly related to the charge transfer impedance of lithium ions at the interface between the electrode and the electrolyte, and the oblique line in the low frequency region is related to the diffusion process of lithium ions in the electrodes.[47] After 200 cycles, the charge transfer resistance of the operated electrodes was slightly increased compared with the fresh electrodes. According to the previous literature,[48] this slight increase was primarily caused by the formation of SEI film. Hollow ZnO/TiO_2 composite sphere electrodes highlighted a low transfer resistance before and after cycling, and exhibited excellent cycling performance due to the unique hollow structure and synergistic effect of ZnO and TiO_2. This could be further verified by the specific capacity variation of hollow ZnO/TiO_2 composite sphere electrodes in a prolonged cycle (Figure 5e). The discharge capacity of hollow ZnO/TiO_2 composite sphere electrodes remained at 709 mA hg^{-1} at current density of 500 mA g^{-1} after 500 cycles.

4. CONCLUSION

In summary, 3D hollow ZnO/TiO_2 composite spheres were successfully constructed via a simple two-step hydrothermal method. The porous hollow sphere structure ensured high specific areas and abundant active sites. The insertion of TiO_2 nanoparticles relieved the drastic fluctuation of ZnO volume

during lithium ion insertion and extraction. 3D hollow ZnO/TiO_2 composite spheres delivered a high electrical conductivity, long-term cycle life, and large reversible capacity. After 500 cycles, the discharge capacity of hollow ZnO/TiO_2 composite spheres was stable at 709 mA h g^{-1} at the current density of 500 mA g^{-1}. At high current density of 1000 mA g^{-1}, their specific capacity remained at 540 mAh g^{-1}.

References

1. A. K. Thakur, R. Prabakaran, M. R. Elkadeem, S. W. Sharshir, M. Arıcı, C. Wang, W. Zhao, J.-Y. Hwang, and R. Saidur, *Journal of Energy Storage*, 32 (2020) 101771.
2. M. Li, J. Lu, Z. Chen, and K. Amine, *Adv Mater.*, (2018) 1800561.
3. M. Armand, and J. M. Tarascon, *Nature*, 451 (2008) 652.
4. Y. Zhao, X. Li, B. Yan, D. Li, S. Lawes, and X. Sun, *Journal of Power Sources*, 274 (2015) 869.
5. V. Etacheri, R. Marom, R. Elazari, G. Salitra, and D. Aurbach, *Energy & Environmental Science*, 4 (2011) 3243.
6. K. Cao, T. Jin, L. Yang, and L. Jiao, *Materials Chemistry Frontiers*, 1 (2017) 2213.
7. F. Zhang, and L. Qi, *Adv Sci (Weinh)*, 3 (2016) 1600049.
8. P. L. Taberna, S. Mitra, P. Poizot, P. Simon, and J. M. Tarascon, *Nat Mater*, 5 (2006) 567.
9. J. Zhu, G. Zhang, X. Yu, Q. Li, B. Lu, and Z. Xu, *Nano Energy*, 3 (2014) 80.
10. C. Liu, X. Zhang, H. Shang, S. Li, Z. Wen, S. Ji, and J. Sun, *Journal of Alloys and Compounds*, 876 (2021) 160113.
11. Z. Zhou, K. Zhang, J. Liu, H. Peng, and G. Li, *Journal of Power Sources*, 285 (2015) 406.
12. Y. Zhang, Y. Lu, S. Feng, D. Liu, Z. Ma, and S. Wang, *Journal of Materials Chemistry A*, 5 (2017) 22512.
13. D. Kim, M. Park, S. M. Kim, H. C. Shim, S. Hyun, and S. M. Han, *ACS Nano*, 12 (2018) 10903.
14. Y. Li, Y. Zhao, G. Huang, B. Xu, B. Wang, R. Pan, C. Men, and Y. Mei, *ACS Appl Mater Interfaces*, 9 (2017) 38522.
15. S. M. Abbas, S. T. Hussain, S. Ali, N. Ahmad, N. Ali, and S. Abbas, *Journal of Materials Science*, 48 (2013) 5429.
16. S. J. Yang, S. Nam, T. Kim, J. H. Im, H. Jung, J. H. Kang, S. Wi, B. Park, and C. R. Park, *J Am Chem Soc*, 135 (2013) 7394.
17. S. Hou, G. Zhang, W. Zeng, J. Zhu, F. Gong, F. Li, and H. Duan, *ACS Appl Mater Interfaces*, 6 (2014) 13564.
18. H. Li, S. Yang, Y. Zhao, T. Tan, X. Wang, and Z. Bakenov, *Journal of Nanomaterials*, 2019 (2019) 1.
19. D. Kim, S. H. R. Shin, Y. Kim, K. Crossley, Y. Kim, H. Han, and J. Yoo, *RSC Advances*, 10 (2020) 13655.
20. G. Wu, Z. Jia, Y. Cheng, H. Zhang, X. Zhou, and H. Wu, *Applied Surface Science*, 464 (2019) 472.
21. H. Liu, W. Li, D. Shen, D. Zhao, and G. Wang, *Journal of the American Chemical Society*, 137 (2015) 150928151626001.

22. W. Li, F. Wang, Y. Liu, J. Wang, J. Yang, L. Zhang, A. A. Elzatahry, D. Al-Dahyan, Y. Xia, and D. Zhao, *Nano Lett*, 15 (2015) 2186.
23. Y. Chen, J. Liang, Q. Tian, W. Zhang, and Z. Sui, *Synthetic Metals*, 263 (2020) 116353.
24. A. R. Ballestas-Barrientos, Q. Xia, A. F. Masters, C. D. Ling, and T. Maschmeyer, *ACS Omega*, 5 (2020) 7584.
25. H. Xie, M. Chen, and L. Wu, *Small*, 13 (2017) 1604283.
26. L. Gao, S. Li, D. Huang, Y. Shen, and M. Wang, *Electrochim. Acta*, 182 (2015) 529.
27. Z. Zhang, P. Xu, H. Zhang, A. Shen, and Y. Zhao, *ACS Applied Energy Materials*, 2 (2019) 5744.
28. Q. Chen, Y. F. Yuan, S. M. Yin, M. Zhu, and G. S. Cai, *Nanotechnology*, 31 (2020) 435410.
29. Y. Q. Cao, S. S. Wang, C. Liu, D. Wu, and A. D. Li, *Sci Rep*, 9 (2019) 11526.
30. H. Han, T. Song, J.-Y. Bae, L. F. Nazar, H. Kim, and U. Paik, *Energy & Environmental Science*, 4 (2011) 4532.
31. Y. Wang, X. Gao, X. Wu, W. Zhang, C. Luo, and P. Liu, *Chemical Engineering Journal*, 375 (2019) 121942.
32. Y. Ren, L. Yang, L. Wang, T. Xu, G. Wu, and H. Wu, *Powder Technology*, 281 (2015) 20.
33. X. Qi, H. Zhang, Z. Zhang, Y. Bian, A. Shen, P. Xu, and Y. Zhao, *Appl. Surf. Sci.*, 452 (2018) 174.
34. H. Gwon, J. Hong, H. Kim, D.-H. Seo, S. Jeon, and K. Kang, Energy Environ Sci., 7 (2019) 538.
35. E. Quartarone, V. Dall'Asta, A. Resmini, C. Tealdi, I. G. Tredici, U. A. Tamburini, and P. Mustarelli, *Journal of Power Sources*, 320 (2016) 314.
36. B. Oschmann, M. N. Tahir, F. Mueller, D. Bresser, I. Lieberwirth, W. Tremel, S. Passerini, and R. Zentel, *Macromol Rapid Commun*, 36 (2015) 1075.
37. C.-T. Hsieh, C.-Y. Lin, Y.-F. Chen, and J.-S. Lin, *Electrochimica Acta*, 111 (2013) 359.
38. Y. Wang, X. Jiang, L. Yang, N. Jia, and Y. Ding, *ACS Appl Mater Interfaces*, 6 (2014) 1525.
39. J. Liu, Y. Li, X. Huang, G. Li, and Z. Li, *Advanced Functional Materials*, 18 (2008) 1448.
40. X. Shen, D. Mu, S. Chen, B. Wu, and F. Wu, *ACS Appl Mater Interfaces*, 5 (2013) 3118.
41. J. Yan, G. Wang, H. Wang, Z. Zhang, X. Ruan, W. Zhao, J. Yun, and M. Xu, *Journal of Nanoparticle Research*, 17 (2015) 52.
42. D. Bresser, F. Mueller, M. Fiedler, S. Krueger, R. Kloepsch, D. Baither, M. Winter, E. Paillard, and S. Passerini, *Chemistry of Materials*, 25 (2013) 4977.
43. N. Garino, A. Lamberti, R. Gazia, A. Chiodoni, and C. Gerbaldi, *Journal of Alloys and Compounds*, 615 (2014) S454.
44. J.-H. Lee, M.-H. Hon, Y.-W. Chung, and I.-C. Leu, *Applied Physics A*, 102 (2010) 545.
45. Yan-Qiang, Cao, Shan-Shan, Wang, Chang, Liu, and Ai-Dong, *Scientific reports*, 9 (2019) 11526.
46. J. Zhao, H. Zhou, M. Jin, P. Chen, S. Chen, and X. Liu, *J. Mater. Sci.*, 56 (2020) 2497.
47. R. Mo, Z. Lei, K. Sun, and D. Rooney, *Adv Mater*, 26 (2014) 2084.
48. G. Liu, X. Yuan, Y. Yang, J. Tao, Y. Chi, L. Hong, Z. Lin, Y. Lin, and Z. Huang, *Journal of Alloys and Compounds*, 780 (2019) 948